Héðinsdalsjökull, northern Iceland: geomorphology recording the recent complex evolution of a glacier

Manuel Rodríguez-Mena, José M. Fernández-Fernández, Luis M. Tanarro, José J. Zamorano & David Palacios

View supplementary material

Published online: 13 May 2021.

Submit your article to this journal

Article views: 138

View related articles

View Crossmark data

Taylor & Francis
Taylor & Francis Group

Science

Héðinsdalsjökull, northern Iceland: geomorphology recording the recent complex evolution of a glacier

Manuel Rodríguez-Mena [a], José M. Fernández-Fernández [a,b], Luis M. Tanarro [a], José J. Zamorano [c] and David Palacios [a]

[a]High Mountain Physical Geography Research Group, Department of Geography, Universidad Complutense de Madrid, Madrid, Spain; [b]Instituto de Geografia e Ordenamento do Território (IGOT), Universidade de Lisboa, Lisbon, Portugal; [c]Instituto de Geografía, Universidad Nacional Autónoma de México, Mexico, Mexico

ABSTRACT

The objective of this work is to conduct a detailed mapping of the Héðinsdalsjökull foreland, northern Iceland (65°39′N, 18°55′W). This cirque currently shows a variety of glacial and periglacial landforms derived from a complex deglaciation. Mapping was performed combining traditional hand-drawn and digital mapping. A hand-drawn sketch was georeferenced in ArcMap 10.7.1, supported on an aerial photograph (year 2000). Its vectorization, symbolization and final design were done in the computer-aided design (CAD) software MicroStation Connect. Complementary high-resolution Digital Surface Models were obtained from historical aerial photographs and ground-view field photographs through the application of Structure from Motion (SfM) photogrammetry. To improve the topographic expression of the geomorphological map, a photorealistic 3D view has been generated. The final map highlights the complexity of the foreland and the coexistence existence of a range of different units and landforms. The map will ease future studies on the transformation of receding glaciers.

1. Introduction

The diversity of landforms that characterize glacial cirques and their clear paleoclimatic significance has been reported in numerous studies, especially in mountain areas that have been glaciated during the Late Pleistocene and deglaciated in the last thousands of years (Barr & Spagnolo, 2015, 2017; Barth et al., 2016; Benedict, 1973; Dahl & Nesje, 1992; Ipsen et al., 2018). Most of the cirque landforms derive from the effects of successive glacial phases (Evans & Cox, 1974, 1995), this does not necessarily imply that these landforms do not continue to evolve after partial or total deglaciation of the cirque. On the contrary, in many cases, the geomorphological evolution of the cirques continues in the following interglacial within the so-called paraglacial phase (Ballantyne, 2002, 2013; Beniston et al., 2018; Knight & Harrison, 2014).

Many of the landforms derived from paraglacial processes transforming cirques are related to the existence of internal frozen masses, e.g. glaciers or ice derived from the existence of permafrost, under vertical walls (Beniston et al., 2018; Jones et al., 2019; Knight & Harrison, 2014; Knight et al., 2019). In fact, paraglacial processes have been considered responsible for an increase of the debris supply onto debris-free glaciers and their transformation into debris-covered glaciers or into rock glaciers (Anderson et al., 2018; Berthling, 2011; Hambrey et al., 2008; Janke et al., 2013, 2015; Jones et al., 2019; Knight et al., 2019; Monnier & Kinnard, 2015, 2016). However, the speed and time required for this transformative process still remains unknown and depends on multiple factors (Anderson et al., 2018; Jones et al., 2019; Knight et al., 2019). An appropriate method to study this transformation is mapping glacier derived landforms and their changes over time (Dusik et al., 2015; Emmer et al., 2015; Monnier & Kinnard, 2015, 2016; Monnier et al., 2014).

The Tröllaskagi peninsula, northern Iceland, is an area with many alpine-type glacial cirques, which host a few debris-free glaciers, and numerous debris-covered glaciers and rock glaciers. For example, Lilleøren et al. (2013) have identified 118 rock glaciers in Tröllaskagi. Debris-free glaciers have been identified as highly sensitive to climate change and with short reaction and response times, with rapid advances or retreats of their fronts that form numerous moraine ridges in their forelands (Caseldine, 1985a, 1985b; Fernández-Fernández et al., 2017, 2019; Häberle, 1991; Kugelmann, 1991). Some debris-covered glaciers and rock glaciers have been studied according to their

---

Table 1. Landforms represented on the geomorphologic map of Héðinsdalsjökull.

Legend of the main map	Clarifications on the origin of the landforms	Typology of landforms
Geomorphological features		
Steep slope discontinuity	Slope	Slope
Scarp		
Debris flow		
Upper glacial trough trim	Erosion	Glacial
Cirque cliff		
Minor collapsed depression with underlying ice	Hummocky landscape	
Major collapse depression with underlying ice		
Collapsed depressions without underlying ice		
Water-filled depression		
Hummocky moraine		
Frontal-lateral push moraine	Moraine ridges	
Big boulder	Erratics	
Ridges and furrows	Rock glacier	Periglacial
Ridges and furrows	Incipient rock glacier derived form a push moraine	Glacial-to-periglacial transition
Glacial and periglacial units	Landform derived from the Neoglacial maximum extent	
Debris-free sector of the glacier in 2000	At present as independent glacier	Present glacier
Margin of the debris-free sector of the glacier in 2019		
Debris-covered sector of the glacier	At present an ice stagnant debris-covered glacier	
Debris-covered marginal zone	A former debris-covered glacier, collapsed after the ice melted away	Glacial landforms
Rock glacier	A former debris-covered glacier, later evolved into a rock glacier	Periglacial
Incipient rock glacier	Incipient rock glacier derived form a push moraine	Glacial-to-periglacial transition
Frontal glacial depression	Depression previously occupied for the front of a glacier	Glacial landforms
Other units		
Plateau	Culminating lava flow surfaces	Structural
Cirque wall		Glacial
Talus cone		Slope
Braided river flood plain		Fluvioglacial
Fluvioglacial terrace		Fluvioglacial

morphology and dynamics, and a number of authors have highlighted their low (or even null) dynamism, especially at rock glaciers, whose main dynamics is by surface subsidence (Andrés et al., 2016; Campos et al., 2019; Martin et al., 1991; Tanarro et al., 2019). Mapping of the Iceland proglacial cirque areas is a first approach to the complex geomorphological evolution that accompanies deglaciation (Evans et al., 2017; Tanarro et al., 2018).

This work addresses with the geomorphological study of the deglaciation of a peculiarly complex alpine cirque, located at the head of a valley in the Tröllaskagi peninsula (Northern Iceland), namely Héðinsdalur. In this cirque and its associated foreland, the coexistence of a current debris-free and debris-covered sectors of the glacier, a debris-covered marginal zone and also a rock glacier have been observed. Thus, the objective of this work is to perform a detailed geomorphological mapping in order to differentiate the phases through which this transformation occurred.

2. Regional setting

This study focuses on the glacier of Héðins (Héðinsdalsjökull in Icelandic), located at the head of the Héðinsdalur (65°39′N, 18°55′W) in western Tröllaskagi. The Tröllaskagi peninsula is located in northern Iceland between the Skagafjörður and Eyjafjörður to the west and east, respectively. The head of the valley connects with the culminating plateau of this peninsula, at altitudes between 1200 and 1330 m a.s.l. The geology of the peninsula is composed of Miocene basaltic lavas (Tertiary Basalt Formation) in a sub-horizontal arrangement, alternating with sedimentary strata (Sæmundsson et al., 1980). Numerous valleys are carved out in this plateau, with steep and unstable slopes, where rock falls, landslides and debris-flows frequently occur (Cossart et al., 2014; Decaulne et al., 2016; Jónsson & Sigvaldason, 1976; Mercier et al., 2013; Sæmundsson et al., 2018; Whalley et al., 1983). Most of the glacier catchments in Tröllaskagi are occupied by debris-covered glaciers and rock glaciers, whose fronts are at altitudes between 900 and 950 m a.s.l., where the mean annual air temperature (MAAT) ranges between −1.8 and −2.6°C (Etzelmüller et al., 2007).

The MAAT on the Tröllaskagi peninsula (1901–1990 series) ranges between 2°C and 4°C at sea level, and between −2°C and −4°C at the summits (Etzelmüller et al., 2007). The lower limit of mountain permafrost in Tröllaskagi is located at ∼900 m a.s.l. (Czekirda et al., 2019; Etzelmüller et al., 2007, 2020; Lilleøren et al., 2013). The mean annual rainfall in the period 1971–2000 ranges from 400 mm in the coastal areas to 2500 mm at the summits (Crochet et al., 2007).

The Héðinsdalsjökull currently shows a number of different morphological zones, namely the present debris-free and the debris-covered sectors of the glacier and a rock glacier. In front of the current glacier

terminus, i.e. the marginal zone, there are sediments of a collapsed debris-covered marginal zone, whose outermost moraine has been dated to 3–2 ka, using [36]Cl cosmic-ray exposure dating (Fernández-Fernández et al., 2020).

3. Methodology

3.1. Analogue geomorphological mapping from aerial photographs and fieldwork

Geomorphological mapping was performed through the interpretation of hard-copy aerial photographs from 1994 (National Land Survey of Iceland) and *in situ* field mapping (Chandler et al., 2018) (See Main map). Mapped landforms were transformed onto a transparent acetate sheet at 1:4,200 scale, with orthophotos from 2000 and 2019 (National Land Survey of Iceland) used as a base map. The hand-drawn map was then scanned at high resolution (600 dpi) for digital processing. We georeferenced the hand-drawn map in ESRI ArcMap 10.8.1 using the UTM grid of the base map as control points. Georeferencing was performed using a 3rd order polynomial transformation, which provided the lowest root mean square error (RMS: 0.33 m) and the best visual fit. The hand-drawn map was then vectorized in the Computer-Aided Design (CAD) software MicroStation Connect, which provided an efficient and intuitive approach to vectorization as well as the capacity to visualize the mapping in 3D. After vectorization, topological errors were corrected using the topology clean-up tools in Bentley Map software.

The main landforms were classified and grouped into geomorphological units (see Table 1). The current limit of the glacier was also drawn based on an aerial photo obtained in 2019 from the online geoviewer Kortasjá/MAP IS (2020), which was also georeferenced with a 3rd order polynomial transformation.

The symbolization and final design of the geomorphological map were performed and carried out in the CAD MicroStation Connect platform. The devised representation system synthesized the graphic style of the geomorphological base map and includes adaptations of widely accepted proposals in geomorphological mapping (Lambiel et al., 2012; Peña Monné et al., 1997; Tricart, 1976). The main elements were custom lines and polygon features to which simple fills and repeating symbol patterns were applied.

In addition, a degree of transparency was applied to the polygon entities in order to highlight the relief shading and to emphasize their topographic expression. The shading was generated from a Digital Elevation Model (DEM) derived from the interpolation of the elevation points and contour lines (20-m interval) for the year 2000 (Icelandic Land Survey, 2020). The final map layout was built in CAD MicroStation Connect.

3.2. 3D model generation from historical aerial photographs

The application of Structure from Motion (SfM) photogrammetric techniques from historical aerial photographs (Chandler et al., 2016; Ewertowski et al., 2019; Gomez, 2012; Gomez et al., 2015; Mertes et al., 2017; Midgley & Tonkin, 2017) was used to obtain a complementary high-resolution digital surface models (DSM) and DEMs. The geomorphological map was draped on the DEM shading in order to apply rendering and lighting techniques and generate 3D views, which considerably improved the understanding and interpretation of the map. In the Bentley ContextCapture photogrammetry software, four aerial photographs of Heðinsdalur, corresponding to the year 1994 (focal length of 152.82 mm; Icelandic Land Survey, 2020) were used to obtain the DEM and the orthophoto. First, in the ArcMap work environment, 13 well-distributed control points were added in the area of interest, easily identifiable with common elements in the 1994 stereo-pairs and the 2000 orthophoto. As a requirement for correct processing of the images, each of the control points was located in at least three of the photographs used. The XYZ coordinates of the control points were obtained in ArcMap, using the orthophoto of the year 2000 (XY coordinates) and the abovementioned DEM (Z coordinate). Then, in Bentley ContextCapture, the control points and their coordinates were entered in at least three different photograms. Next, the aerial triangulation and alignment of the photographs were carried out, from which the 3D model was obtained. In this process, the global 3D RMS error was 5.7 m. Finally, the DEM (in Ascii grid format) and the orthophoto (in GeoTiff format) were produced, at a default spatial resolution of 0.45 m.

To improve geovisualization of the geomorphology in the study area, a photorealistic 3D view of the geomorphological map was generated using the 3D tools of the CAD MicroStation Connect through the application of rendering techniques and solar lighting (Tanarro et al., 2018). This required the elaboration of a polygonal mesh from a point cloud, which was previously derived from 3D photo-reconstruction. Finally, the geomorphological map was draped on the polygon mesh in a three-dimensional view.

One of the advantages of CAD software is the realism of its views thanks to the rendering tools, which allow for configuration of the illumination settings and drape the map on the 3D mesh as a texture. In this case, the solar position was established based on the coordinates of the study site, on 17 July 2020 at 03:30 GMT.

3.3. 3D model generation from ground-view field photographs

The SfM technique was used complementarily as being capable of obtaining high-resolution 3D

cartographic products in a simple way and at very low cost (Micheletti et al., 2014). The Bentley Context Capture photogrammetry software was also used to process 43 terrestrial photographs of a section of the southern slope of Heðinsdalur, taken on 30 August 2018 from the opposite slope, and at a distance between 500 and 1300 m from the photographed landforms. This section coincides with the sector occupied by the glacier during the Neoglacial maximum advance (Fernández-Fernández et al., 2020). From this technique, we produced a DSM and an orthophoto of the lower sector of the debris mantle located in the marginal zone, with a resolution higher (0.27 m) compared to that of the aerial photographs. In fact, the derived stereo-orthophoto greatly helped to recognize and map the chaotic collapsed landforms of this sector. The photographs were taken with the integrated camera of a GPS Garmin Monterra, with a focal length of 4.6 mm and 8 megapixels (3266 × 2450 pixels) of resolution. In this case, the identification of control points was not necessary since the photographs were already geolocated by default (Micheletti et al., 2015).

4. Results

4.1. Glacial and periglacial landforms

The geomorphological map obtained in this work distinguishes different units, defined as present debris-free and debris-covered sectors of the glacier, a debris-covered marginal zone and a rock glacier, all of them within the same cirque. Considering that the outermost moraines date to about 3–2 ka (Fernández-Fernández et al., 2020), the recent evolution of Héðinsdalsjökull has been rapid. The obtained cartography offers a more realistic and expressive appearance in a three-dimensional view (Figures 1–3, Table 1).

4.1.1. Debris-free sector of the glacier

The current debris-free glacier sector is located at the head of the valley (Figures 1–4). With data from the year 2000, this glacier had an area of 4.9 km^2 (2.3 km long and 2.6 km wide), while in 2019, its surface had been slightly reduced (to 4.7 km^2). The glacier ends in a wide front, of 3.1 km long and located between 1040 and 900 m a.s.l.. The westernmost part of this debris free glacier terminus is covered by a thin layer of debris <0.5 m thick. Towards the center and east, the debris cover disappears and the front of the glacier is completely debris-free, which coincides with the areas where there was a greater retreat between 2000 and 2019, as happened in the nearby debris-free glacier Western Tungnahryggsjökull (Fernández-Fernández et al., 2019).

4.1.2. Active debris-covered sector of the glacier

The terminus of the debris-free sector of the glacier overlaps an underlying debris-covered stagnant sector of the glacier, with a dense layer of supraglacial debris (Figures 1–5). This unit has been characterized and classified as a debris-covered glacier on the basis on: the supraglacial debris mantle covers ≥50% of the ablation area, with a thickness of >0.5 m, a predominance of ridges longitudinal to the glacier flow and the presence of lateral moraines (Azócar & Brenning, 2010; Brenning, 2005; Hambrey et al., 2008; Kirkbride, 2000, 2011; Monnier & Kinnard, 2015). This debris-covered glacier has an area of 1.2 km^2 with an altitudinal range between 1080 and 700 m a.s.l.

Apart from the longitudinal ridges and moraines, collapse depressions are also abundant. Differentiation has been made between major collapse depressions, with almost vertical walls, and minor collapsed depressions, with gentle slopes. Some of these depressions are water-filled, which explains their small-lake-type appearance. Between these depressions there are many mounds and small moraine hills, of chaotic morphology.

The general morphology of the active debris-covered sector of the glacier is dominated by thermokarst-like features. Moreover, sections of frontal or fronto-lateral moraine arches of different morphology and sizes are preserved and allow for differentiation at four stages of advance or stabilization of the glacier front.

The central axis of the debris-covered sector of the glacier is reworked by meltwater stream and tends to erode all the glacial and collapse-derived landforms described above.

Other active debris-covered glaciers have been studied in nearby Tröllaskagi cirques, such as Hóladalsjökull (Tanarro et al., 2018, 2019) and Hofsjökull (Campos et al., 2019). From a morphological point of view, Héðinsdalsjökull differs from them by the much higher density of collapse depressions and the limited preservation of moraine landforms.

4.1.3. Incipient rock glacier (proto-rock glacier)

Inside the active debris-covered glacier there is a sector characterized by having an abrupt front and the predominance of ridges and furrows parallel to each other and perpendicular to the flow. Although this sector is within the active debris-covered glacier, it has been interpreted as a developing of a rock glacier or 'proto-rock glacier', based on the abovementioned features (Figures 1–3 and 6). Incipient rock glaciers have also been detected in some nearby Tröllaskagi cirques, as in the Fremri-Grjótárdalur cirque (Tanarro et al., 2018, 2019) (Figure 7).
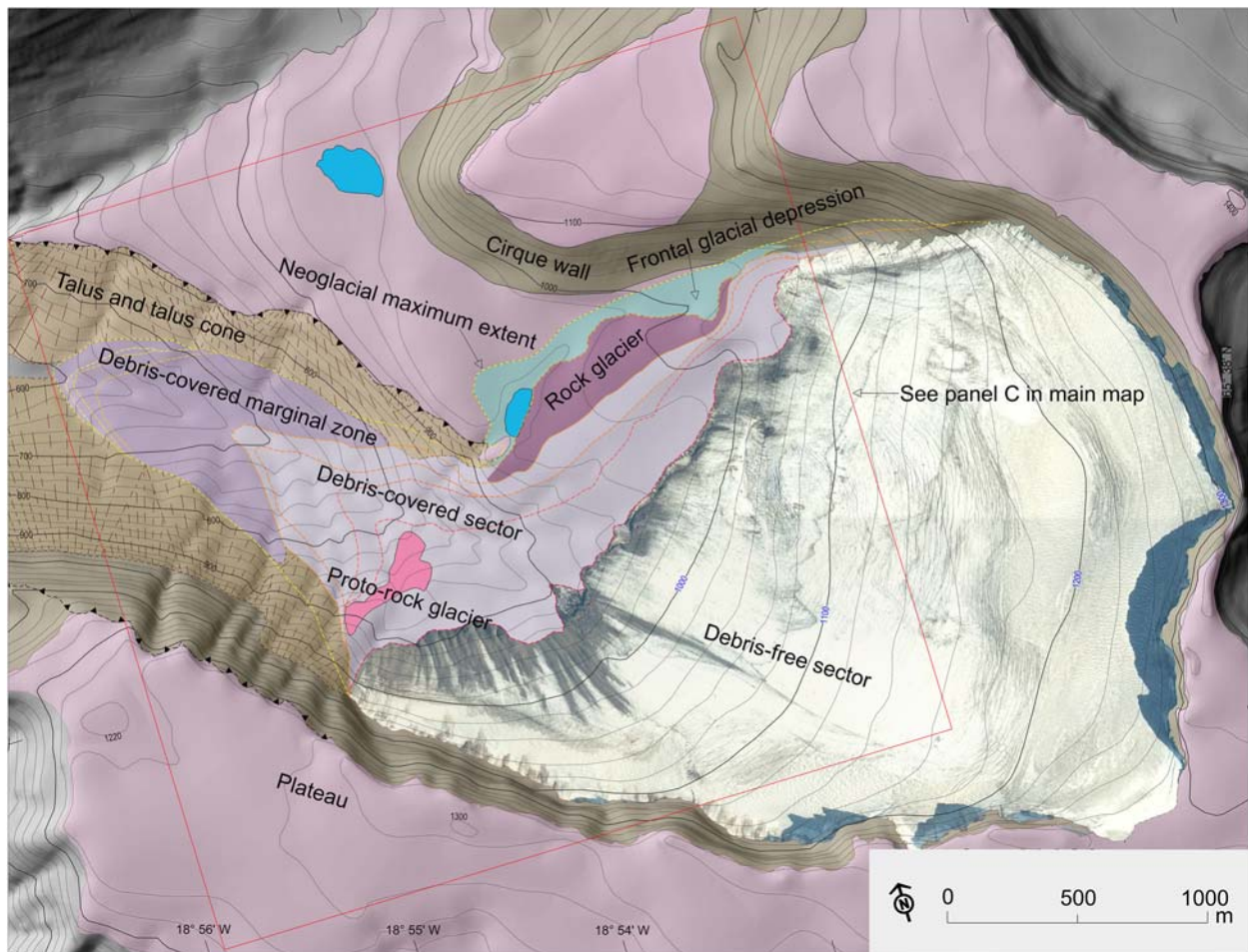
Figure 1. Main geomorphological units of Héðinsdalsjökull: debris-covered marginal zone (without glacial ice); debris-covered sector (with underlying stagnant glacial ice), rock glacier and debris-free sector. The limit of the last Neoglacial advance is indicated according to Fernández-Fernández et al. (2020).

4.1.4. Debris-covered marginal zone

Ahead of the active debris-covered sector of the glacier are the deposits of a former debris-covered glacier, currently collapsed due to the complete melting of the subglacial ice (Figures 1–3 and 8). This unit descends from 820 m a.s.l. in its upper part up to 600 m a.s.l.in the former frontal area.

Within the debris-covered marginal zone, collapse depressions and melt depressions predominate. Their flat-bottomed appearance denotes the absence of ice at their base. Moraines are also common in this sector, showing different morphologies, with a predominance of ridges longitudinal to the flow. The moraine ridges on the front have been dated through

Figure 2. Three-dimensional view of the Héðinsdalsjökull (orthophoto from year 2000) and main geomorphological units.
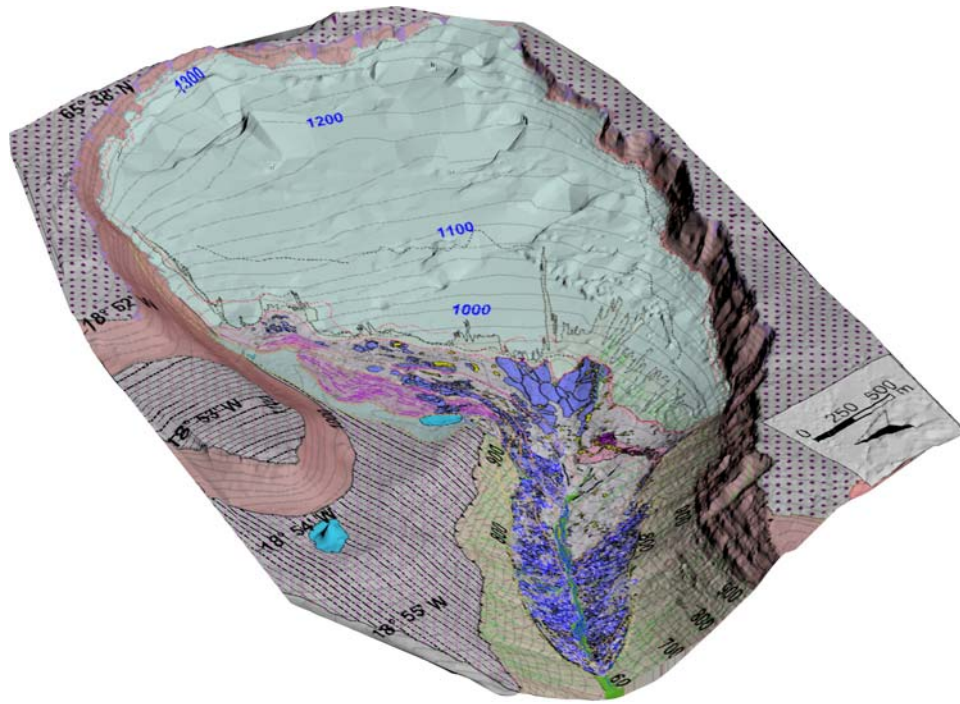
Figure 3. Three-dimensional view of the geomorphological map of Héðinsdalsjökull and main geomorphological units. The reader is referred to the main map symbology for the identification of the units.

the ³⁶Cl cosmonuclide to 3–2 ka, and interpreted as the date of their final stabilization (Fernández-Fernández et al., 2020). This advance coincides with clear Neoglacial advances of other debris-free glaciers, such as Tungnahryggsjökull (Fernández-Fernández et al., 2019). In addition to these moraine ridges, small moraine mounds or hills are very abundant, contributing to a hummocky moraine landscape (Grindvik-Knudsen et al., 2006).

The landforms of the debris-covered marginal zone are affected by a braided stream that drains the melt waters of the glacier and has reshaped the entire central axis of this geomorphological unit as it has already been observed in other cases (Janke et al., 2013; Monnier & Kinnard, 2016).

4.1.5. Rock glacier

Facing the NE of Héðinsdalsjökull and resting on a platform at 1000 m a.s.l., a rock glacier extends, with its characteristic morphology of steep front and surface boulders arranged in parallel ridges and furrows, perpendicular to the flow (Figures 1–3 and 9). Although the collapse depressions are rare, in some of them the great thickness of the debris cover and the proportion of interstitial ice can be observed.

The rock glacier covers an area of 0.2 km², with a maximum length and width of 1.2 km and 245 m, respectively. This formation has its root at 1020 m a.s.l., and descends to the minimum elevation of 920 m a.s.l., with an average slope of 10.9%. Its front reaches a depression occupied by a small lake (0.01 km²).

In similar rock glaciers, located in nearby cirques and at similar altitudes, ice has been detected below a dense layer of debris 2–3 m thick (Andrés et al., 2016; Campos et al., 2019; Farbrot et al., 2007; Kellerer-Pirklbauer et al., 2007; Tanarro et al., 2019; Wangensteen et al., 2006).

4.1.6. Frontal-glacial depression

In front of the rock glacier there is a frontal-glacial depression dotted with erratic boulders. In the outermost sector of the depression, the erratic boulders are aligned and delimit the maximum glacial advance that closed this depression (Figure 9).

4.1.7. Glacier cirque and scarps

The head of Héðinsdalur presents the characteristic morphology of a glacial cirque (Figures 1–4), which is semi ellipsoidal and with steep slopes. The walls of the cirque delimit the glacier at its upper end and occupy an area of 2.5 km², with altitudes between 1360 and 960 m. These bedrock walls are characterized by an almost vertical inclination in some sections, especially at the head of the glacier and in the southern part.

4.2. Other landforms

The cirque is carved out on a plateau summit, at altitudes between 1180 and 1400 m a.s.l. These surfaces are covered by patterned ground, which evidences the presence of active permafrost. At the NE of Héðinsdalsjökull, there is an intermediate plain, at
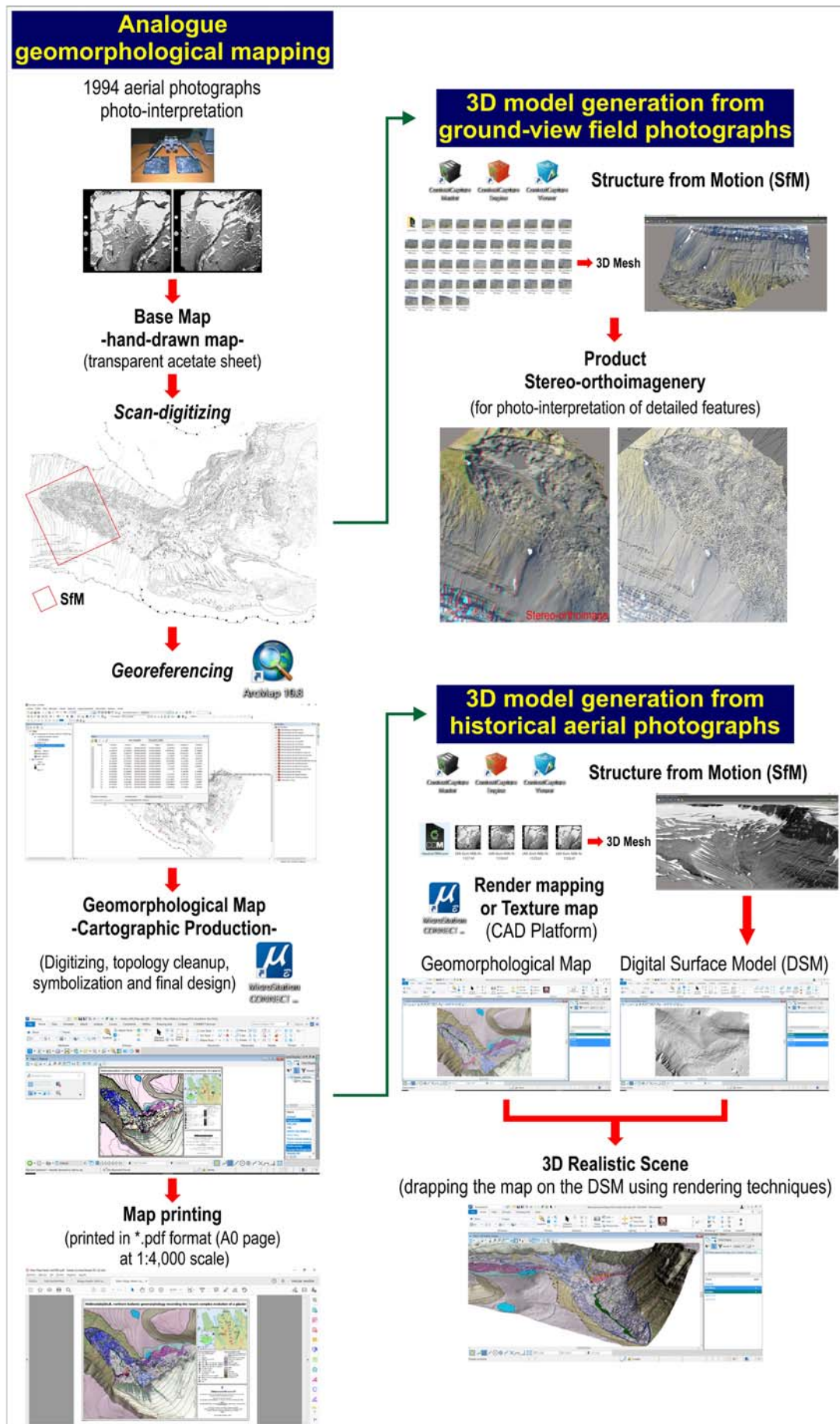
Figure 4. Workflow including the different steps for the production and visualization of the geomorphological map of Héðinsdalsjökull.
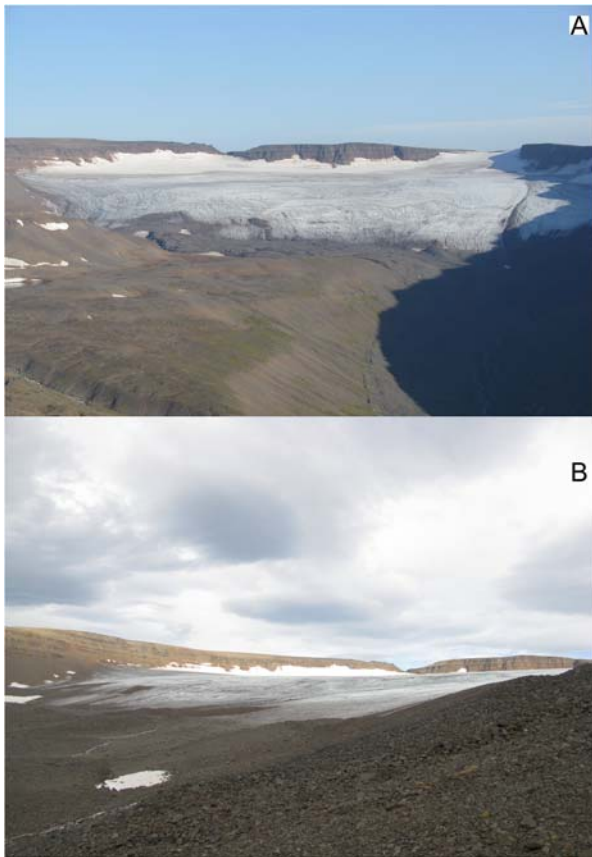
Figure 5. Headwall of Héðinsdalsjökull cirque (August, 2018). (A) Héðinsdalsjökull viewed from the north. The rock glacier can be seen ahead of the debris-free glacier on the lower platform. (B) Héðinsdalsjökull viewed from the west.

Figure 6. Debris-covered sector of Héðinsdalsjökull. (A) The debris-covered sector extends between the debris-free sector and the marginal debris-covered zone. (B) The thickness of the debris mantle and the underlying stagnant glacial ice can be seen in numerous collapse depressions.

altitudes of 1080–1160 m a.s.l. Below this, there is a lower one, with lower altitudes, between 1040 and 760 m a.s.l. The NE sector of the rock glacier rests on the latter surface.

Rockfall talus is deposited on the cirque walls in the south and in the northern lower plain. This unit occupies an area of 1.1 km^2, with an average slope of 62.6%. On the rock fall talus numerous debris flow are formed. These debris flows usually begin at the limit that separates the talus and the walls of the cirque. Their lengths range from 400 to 200 m, although some can be >800 m along slopes of 60%. A fluvioglacial plain, rises in front of the collapsed debris-covered glacier from 600 m a.s.l.

5. Conclusions

The combination of field surveys, detailed traditional cartographical techniques, the application of tools based on the latest photogrammetry techniques, and different software allowed obtaining cartographical products, that show great graphic expressiveness and transmit a large amount of information. In this sense, the use of CAD software stands out as an efficient tool both for map vectorization and visualization. In addition, the use of
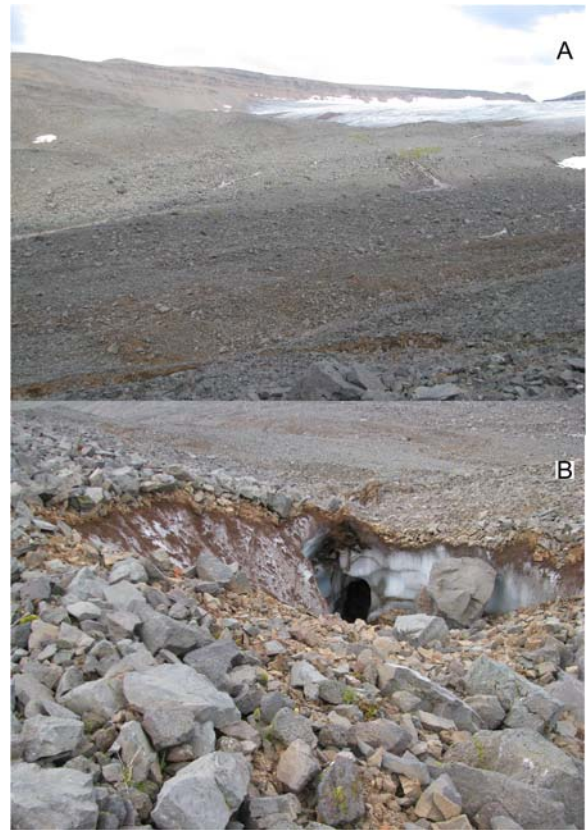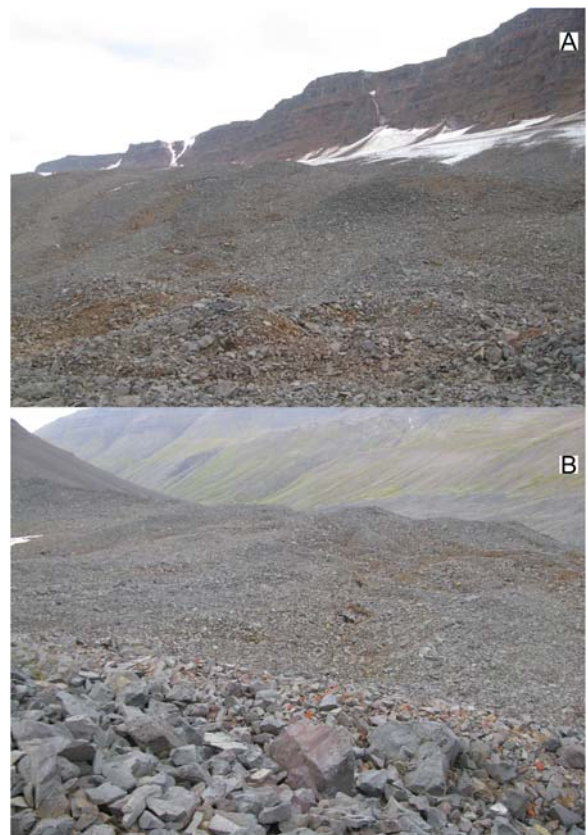

Figure 7. Proto-rock glacier on the debris-covered sector. (A) View from the front. (B) View from the upper part.
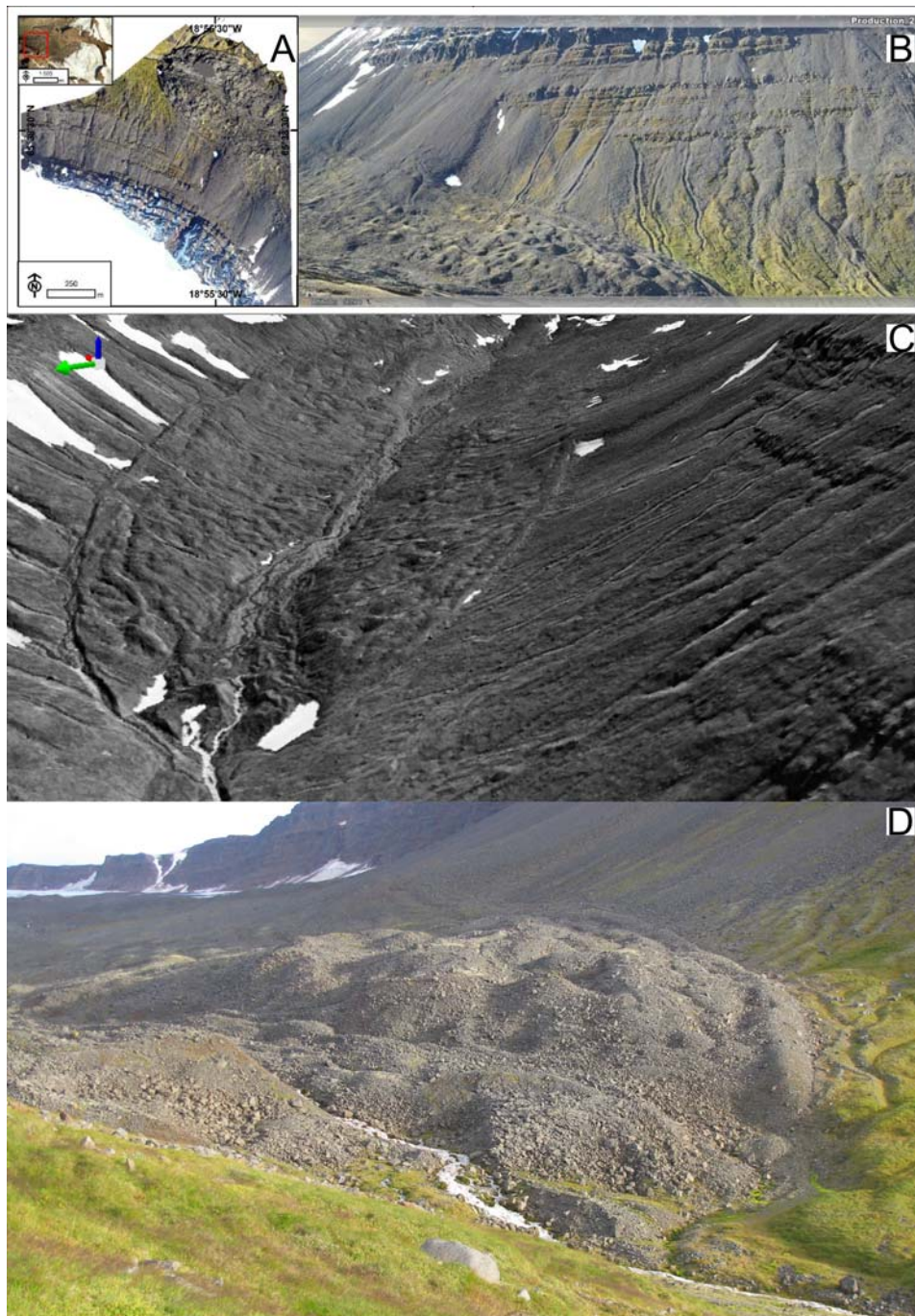
Figure 8. Debris-covered marginal zone, outermost ridges and the hummocky moraine landscape. (A) High resolution orthophoto obtained from SfM. (B) Oblique view from the east. (C) 3D oblique view of the reconstructed orthophoto from the north. (D) Front viewed from the north.

realistic 3D isometric view obtained through SfM photogrammetry techniques based on aerial photography and field photographs allows the most complex areas to be analyzed and displayed remotely with greater clarity.

This work provides a map of the Hédinsdalur cirque and foreland at 1:4000 scale. The detailed geomorphological map allows differentiating several units within the Héðinsdalsjökull complex, and highlights the existence of different types of large units related to icy formations within an evolution continuum of debris-free glacier, active debris-covered glacier, collapsed debris-covered glacier and rock glacier. The landforms inside the large units are used to classify them as moraines, hummocky moraines, ridges, furrows and the different collapse landforms. In addition, the gravitational slope landforms are also highlighted, such as talus and debris flows, which reworked the interior of the glacier complex by destroying or covering glacial landforms, and consequently, have influenced its evolution. In fact, these slope processes still influence the evolution of the debris-free glacier, supplying debris to its front and slowing down its retreat during recent decades.
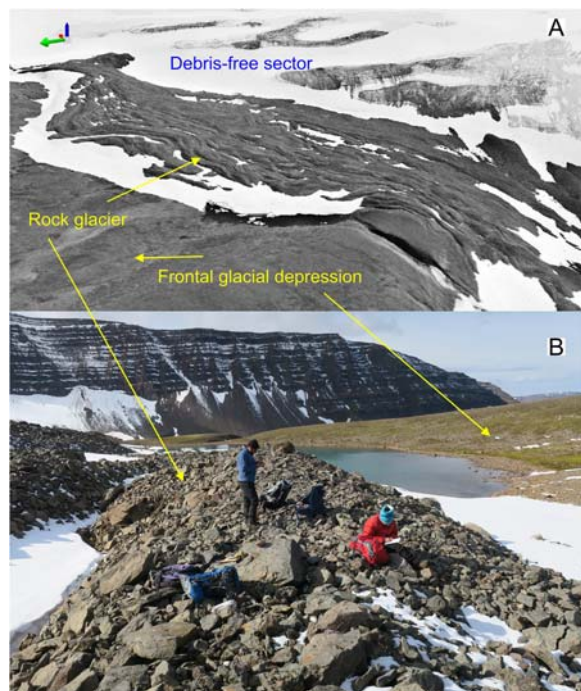
Figure 9. Rock glacier. (A) 3D oblique view of the reconstructed orthophoto from the north-east. (B) Front, lake and frontal glacial depression head of it.

The information provided by the map will improve subsequent studies on the evolution of glaciers in paraglacial environments. The continuous contribution of debris from the cirque walls can transform a debris-free glacier into a debris-covered glacier, to end up transforming into a rock glacier. These different phases have usually been identified in different cirques and the process of evolution has been deduced and modeled, but this transformation has rarely been observed. The contribution of the Héðinsdalsjökull map is that all these phases have occurred in the same glacier and in a very short time, for 2–3 ka. The different genetic units outlined in the map reveal a number of evolutionary phases. First there was a debris-covered glacier, which melted and completely collapsed, although above 700 m a.s.l., an active debris-covered glacier still survives. Then, above 900 m a.s.l. a rock glacier was formed, and finally the front of the debris-free sector overlapped, and still does, the debris-covered sector of glacier, that remains stagnant. The map provides this valuable information for further investigation on the chronology and processes involved in these phases.

The glacier complex of Héðinsdalsjökull continues to evolve, under intense slope processes and the effects of present climate change. The final map constitutes an important source of information to establish the magnitude of future changes within this complex.

Software

We used the ArcGIS 10.8.1 (ESRI) to georeference the base map and the CAD Bentley MicroStation Connect Edition to vectorize the geomorphological features and units and to create the 3D geovisualization of the map. We used the photogrammetry software Bentley Context Capture to create SfM products. Bentley map was used to fix the topology. Also, we produced the final composition and graphic design of the geomorphological map using MicroStation Connect.

Disclosure statement

No potential conflict of interest was reported by the author(s).

Data availability statement

The authors confirm that the data supporting the findings of this study are available within the article and its supplementary materials.

ORCID

Manuel Rodríguez-Mena 🆔 http://orcid.org/0000-0003-3542-3591
José M. Fernández-Fernández 🆔 http://orcid.org/0000-0002-6948-1530
Luis M. Tanarro 🆔 http://orcid.org/0000-0003-0871-7711
José J. Zamorano 🆔 http://orcid.org/0000-0002-9575-5734
David Palacios 🆔 http://orcid.org/0000-0002-8289-0398

References

Anderson, R. S., Anderson, L. S., Armstrong, W. H., Rossi, M. W., & Crump, S. E. (2018). Glaciation of alpine valleys: The glacier–debris-covered glacier–rock glacier continuum. *Geomorphology*, *311*, 127–142. https://doi.org/10.1016/j.geomorph.2018.03.015

Andrés, N., Palacios, D., Tanarro, L. M., & Fernández, J. M. (2016). The origin of glacial alpine landscape in Tröllaskagi peninsula (North Iceland). *Cuadernos de Investigación Geográfica*, *42*(2), 341–368. https://doi.org/10.18172/cig.2935

Azócar, G., & Brenning, A. (2010). Hydrological and geomorphological significance of rock glaciers in the dry Andes, Chile. *Permafrost and Periglacial Processes*, *21*(1), 42–53. https://doi.org/10.1002/ppp.669

Ballantyne, C. K. (2002). Paraglacial geomorphology. *Quaternary Science Reviews*, *21*(18–19), 1935–2017. https://doi.org/10.1016/S0277-3791(02)00005-7

Ballantyne, C. K. (2013). Paraglacial geomorphology. In S. A. Elias (Ed.), *Encyclopedia of quaternary science* (pp. 553–565). Elsevier. https://doi.org/10.1016/B978-0-444-53643-3.00089-3

Barr, I. D., Ely, J. C., Spagnolo, M., Clark, C. D., Evans, I. S., Pellicer, X. M., Pellitero, R., & Rea, B. R. (2017). Climate patterns during former periods of mountain glaciation in Britain and Ireland: Inferences from the cirque record. *Palaeogeography, Palaeoclimatology, Palaeoecology*, *485*, 466–475. https://doi.org/10.1016/j.palaeo.2017.07.001

Barr, I. D., & Spagnolo, M. (2015). Glacial cirques as palaeoenvironmental indicators: Their potential and limitations. *Earth Science Reviews*, *151*, 48–78. https://doi.org/10.1016/j.earscirev.2015.10.004

Barth, A. M., Clark, P. U., Clark, J., McCabe, A. M., & Caffee, M. (2016). Last Glacial Maximum cirque glaciation in Ireland and implications for reconstructions of the Irish Ice Sheet. *Quaternary Science Reviews*, *141*, 85–93. https://doi.org/10.1016/j.quascirev.2016.04.006

Benedict, J. B. (1973). Chronology of cirque glaciation, Colorado front range. *Quaternary Research*, *3*(4), 584–599. https://doi.org/10.1016/0033-5894(73)90032-X

Beniston, M., Farinotti, D., Stoffel, M., Andreassen, L. M., Coppola, E., Eckert, N., Fantini, A., Giacona, F., Hauck, C., Huss, M., Huwald, H., Lehning, M., López-Moreno, J. I., Magnusson, J., Marty, C., Moran-Tejéda, E., Morin, S., Naaim, M., Provenzale, A., … Vincent, C. (2018). The European mountain cryosphere: A review of its current state, trends, and future challenges. *Cryosphere*, *12*(2), 759–794. https://doi.org/10.5194/tc-12-759-2018

Berthling, I. (2011). Beyond confusion: Rock glaciers as cryo-conditioned landforms. *Geomorphology*, *131*(3-4), 98–106. https://doi.org/10.1016/j.geomorph.2011.05.002

Brenning, A. (2005). Geomorphological, hydrological and climatic significance of rock glaciers in the Andes of Central Chile (33–35 degrees S). *Permafrost and Periglacial Processes*, *16*(3), 231–240. https://doi.org/10.1002/ppp.528

Campos, N., Tanarro, L. M., Palacios, D., & Zamorano, J. J. (2019). Slow dynamics in debris-covered and rock glaciers in Hofsdalur, Tröllaskagi Peninsula (northern Iceland). *Geomorphology*, *342*, 61–77. https://doi.org/10.1016/j.geomorph.2019.06.005

Caseldine, C. J. (1985a). Survey of Gljúfurárjökull and features associated with a glacier burst in Gljúfurárdalur, Northern Iceland. *Jökull*, *35*, 61–68. http://jokulljournal.is/21-39/1985/061.pdf

Caseldine, C. J. (1985b). The extent of some glaciers in Northern Iceland during the Little Ice Age and the nature of recent deglaciation. *The Geographical Journal*, *151*(2), 215–227. https://doi.org/10.2307/633535

Chandler, B. M. P., Evans, D. J. A., Roberts, D. H., Ewertowski, M., & Clayton, A. I. (2016). Glacial geomorphology of the Skálafellsjökull foreland, Iceland: A case study of 'annual' moraines. *Journal of Maps*, *12*(5), 904–916. https://doi.org/10.1080/17445647.2015.1096216

Chandler, B. M. P., Lovell, H., Boston, C. M., Lukas, S., Barr, I. D., Benediktsson, ÍÖ, Benn, D. I., Clark, C. D., Darvill, C. M., Evans, D. J. A., Ewertowski, M. W., Loibl, D., Margold, M., Otto, J.-C., Roberts, D. H., Stokes, C. R., Storrar, R. D., & Stroeven, A. P. (2018). Glacial geomorphological mapping: A review of approaches and frameworks for best practice. *Earth-Science Reviews*, *185*, 806–846. https://doi.org/10.1016/j.earscirev.2018.07.015

Cossart, E., Mercier, D., Decaulne, A., Feuillet, T., Jónsson, H. P., & Saemundsson, Þ. (2014). Impacts of post-glacial rebound on landslide spatial distribution at a regional scale in northern Iceland (Skagafjörður). *Earth Surface Processess and Landforms*, *39*(3), 336–350. https://doi.org/10.1002/esp.3450

Crochet, P., Jóhannesson, T., Jónsson, T., Sigurðsson, O., Björnsson, H., Pálsson, F., & Barstad, I. (2007). Estimating the spatial distribution of precipitation in Iceland using a linear model of orographic precipitation. *Journal of Hydrometeorology*, *8*(6), 1285–1306. https://doi.org/10.1175/2007JHM795.1

Czekirda, J., Westermann, S., Etzelmüller, B., & Jóhannesson, T. (2019). Transient modelling of permafrost distribution in Iceland. *Frontiers in Earth Science*, *7*. https://doi.org/10.3389/feart.2019.00130

Dahl, S. O., & Nesje, A. (1992). Palaeoclimatic implications based on equilibrium-line altitude depressions of reconstructed Younger Dryas and Holocene cirque glaciers in inner Nordfjord, western Norway. *Palaeogeography, Palaeoclimatology, Palaeoecology*, *94*(1–4), 87–97. https://doi.org/10.1016/0031-0182(92)90114-K

Decaulne, A., Cossart, E., Mercier, D., Feuillet, T., Coquin, J., & Jónsson, H. P. (2016). An early Holocene age for the Vatn landslide (Skagafjörður, central northern Iceland): Insights into the role of postglacial landsliding on slope development. *The Holocene*, *26*(8), 1304–1318. https://doi.org/10.1177/0959683616638432

Dusik, J. M., Leopold, M., Heckmann, T., Haas, F., Hilger, L., Morche, D., Neugirg, F., & Becht, M. (2015). Influence of glacier advance on the development of the multipart Riffeltal rock glacier, Central Austrian Alps. *Earth Surface Processes and Landforms*, *40*(7), 965–980. https://doi.org/10.1002/esp.3695

Emmer, A., Loarte, E. C., Klimes, J., & Vilímek, V. (2015). Recent evolution and degradation of the bent Jatunraju glacier (Cordillera Blanca, Peru). *Geomorphology*, *228*, 345–355. https://doi.org/10.1016/j.geomorph.2014.09.018

Etzelmüller, B., Farbrot, H., Guðmundsson, Á, Humlum, O., Tveito, O. E., & Björnsson, H. (2007). The regional distribution of mountain permafrost in Iceland. *Permafrost and Periglacial Processes*, *18*(2), 185–199. https://doi.org/10.1002/ppp.583

Etzelmüller, B., Patton, H., Schomacker, A., Czekirda, J., Girod, L., Hubbard, A., Lilleøren, K. S., & Westermann, S. (2020). Icelandic permafrost dynamics since the Last Glacial Maximum – Model results and geomorphological implications. *Quaternary Science Reviews*, *233*, 106236. https://doi.org/10.1016/j.quascirev.2020.106236

Evans, I. S., & Cox, N. J. (1974). Geomorphometry and the operational definition of cirques. *Area*, *6(2)*, 150–153. http://www.jstor.org/stable/20000855

Evans, I. S., & Cox, N. J. (1995). The form of glacial cirques in the English Lake District, Cumbria. *Zeitschrift für Geomorphologie*, *39*(2), 175–202. https://doi.org/10.1127/zfg/39/1995/175

Evans, D. J., Ewertowski, M., & Orton, C. (2017). Skaftafellsjökull, Iceland: Glacial geomorphology recording glacier recession since the Little Ice Age. *Journal of Maps*, *13*(2), 358–368. https://doi.org/10.1080/17445647.2017.1310676

Ewertowski, M. W., Evans, D. J. A., Roberts, D. H., Tomczyk, A. M., Ewertowski, W., & Pleksot, K. (2019). Quantification of historical landscape change on the foreland of a receding polythermal glacier, Hørbyebreen, Svalbard. *Geomorphology*, *325*, 40–54. https://doi.org/10.1016/j.geomorph.2018.09.027

Farbrot, H., Etzelmuller, B., Guðmundsson, A., Humlum, O., Kellerer-Pirklbauer, A., Eiken, T., & Wangensteen, B. (2007). Rock glaciers and permafrost in Trollaskagi, northern Iceland. *Zeitschrift fur Geomorphologie*, *51*(2), 1–16. https://doi.org/10.1127/0372-8854/2007/0051S2-0001

Fernández-Fernández, J. M., Andrés, N., Sæmundsson, Þ, Brynjólfsson, S., & Palacios, D. (2017). High sensitivity of North Iceland (Tröllaskagi) debris-free glaciers to climatic change from the "Little Ice Age" to the present. *The Holocene*, *27*(8), 1187–1200. https://doi.org/10.1177/0959683616683262

Fernández-Fernández, J. M., Palacios, D., Andrés, N., Schimmelpfennig, I., Brynjólfsson, S., Sancho, L. G., Zamorano, J. J., Heiðmarsson, S., & Sæmundsson, Þ. (2019). A multi-proxy approach to Late Holocene fluctuations of Tungnahryggsjökull glaciers in the Tröllaskagi peninsula (northern Iceland). *Science of The Total Environment*, *664*, 499–517. https://doi.org/10.1016/j.scitotenv.2019.01.364

Fernández-Fernández, J. M., Palacios, D., Andrés, N., Schimmelpfennig, I., Tanarro, L. M., Brynjólfsson, S., López-Acevedo, F. J., Sæmundsson, Þ, & Team, A. S. T. E. R. (2020). Constrains on the timing of debris-covered and rock glaciers: An exploratory case study in the Hólar área, nothern Iceland. *Geomorphology*, *361*, 107–196. https://doi.org/10.1016/j.geomorph.2020.107196

Gomez, C. (2012). Historical 3D topographic reconstruction of the Iwaki Volcano using structure from motion from uncalibrated aerial photographs. https://hal.archives-ouvertes.fr/hal-00765723

Gomez, C., Hayakawa, Y., & Obanawa, H. (2015). A study of Japanese landscapes using structure from motion derived DSMs and DEMs based on historical aerial photographs: New opportunities for vegetation monitoring and diachronic geomorphology. *Geomorphology*, *242*, 11–20. https://doi.org/10.1016/j.geomorph.2015.02.021

Grindvik-Knudsen, C., Larsen, E., Sejrup, H. P., & Stalsberg, K. (2006). Hummocky moraine landscape on Jæren, SW Norway – Implications for glacier dynamics during the last deglaciation. *Geomorphology*, *77*(1-2), 153–168. https://doi.org/10.1016/j.geomorph.2005.12.011

Häberle, T. (1991). Holocene glacial history of the Hörgádalur area, Tröllaskagi, northern Iceland. In J. K. Maizels, & C. Caseldine (Eds.), *Environmental change in Iceland: Past and present* (pp. 193–202). Kluwer Academic Publishers. https://doi.org/10.1007/978-94-011-3150-6_13

Hambrey, M. J., Quincey, D. J., Glasser, N. F., Reynolds, J. M., Richardson, S. J., & Clemmens, S. (2008). Sedimentological, geomorphological and dynamic context of debris-mantled glaciers, Mount Everest (Sagarmatha) region, Nepal. *Quaternary Science Reviews*, *27*(25–26), 2361–2389. https://doi.org/10.1016/j.quascirev.2008.08.010

Icelandic Meteorological Office. (2020). Climatological data. Retrieved October 13, 2020 from: http://en. vedur.is/ climatology/data/

Ipsen, H. A., Principato, S. M., Grube, R. E., & Lee, J. F. (2018). Spatial analysis of cirques from three regions of Iceland: Implications for cirque formation and palaeoclimate. *Boreas*, *47*(2), 565–576. https://doi.org/10.1111/bor.12295

Janke, J. R., Bellisario, A. C., & Ferrando, F. A. (2015). Classification of debris-covered glaciers and rock glaciers in the Andes of central Chile. *Geomorphology*, *241*, 98–121. https://doi.org/10.1016/j.geomorph.2015.03.034

Janke, J. R., Regmi, N. R., Giardino, J. R., & Vitek, J. D. (2013). Rock glaciers. In J. Shroder, R. Giardino, & J. Harbor (Eds.), *Treatise on geomorphology. Vol. 8: Glacial and periglacial geomorphology* (pp. 238–273). Academic Press. https://doi.org/10.1016/B978-0-12-374739-6.00211-6

Jones, D. B., Harrison, S., & Anderson, K. (2019). Mountain glacier-to-rock glacier transition. *Global and Planetary Change*, *181*, 102999. https://doi.org/10.1016/j.gloplacha.2019.102999

Jónsson, ÓB, & Sigvaldason, J. (1976). *Berghlaup*. Ræktunarfélag Norðurlands.

Kellerer-Pirklbauer, A., Wangensteen, B., Farbrot, H., & Etzelmüller, B. (2007). Relative surface age-dating of rock glacier systems near Hólar in Hjaltadalur, Northern Iceland. *Journal of Quaternary Science*, *23*(2), 137–151. https://doi.org/10.1002/jqs.1117

Kirkbride, M. P. (2000). Ice-marginal geomorphology and Holocene expansion of debris-covered Tasman glacier, New Zealand. In M. Nakawo, C. F. Raymond, & A. Fountain (Eds.), *Debris covered glaciers* (pp. 211–217). IAHS. http://hydrologie.org/redbooks/a264/iahs_264_0211.pdf

Kirkbride, M. P. (2011). Debris-covered glaciers. In V. Singh, P. Singh, & U. K. Haritashya (Eds.), *Encylopedia of Snow, Ice and Glaciers: Encyclopedia of Earth Series* (pp. 180–182). Netherlands: Springer. https://doi.org/10.1007/978-90-481-2642-2_622

Knight, J., & Harrison, S. (2014). Mountain glacial and paraglacial environments under global climate change: Lessons from the past, future directions and policy implications. *Geografiska Annaler: Series A, Physical Geography*, *96*(3), 245–264. https://doi.org/10.1111/geoa.12051

Knight, J., Harrison, S., & Jones, D. B. (2019). Rock glaciers and the geomorphological evolution of deglacierizing mountains. *Geomorphology*, *324*, 14–24. https://doi.org/10.1016/j.geomorph.2018.09.020

Kugelmann, O. (1991). Dating recent glacier advances in the Svarfadardalur-Skíðadalur area of Northern Iceland by means of a new lichen curve. In J. K. Maizels, & C. Caseldine (Eds.), *Environmental change in Iceland: Past and present* (pp. 203–217). Springer Netherlands. https://doi.org/10.1007/978-94-011-3150-6_14

Lambiel, C., Maillard, B., Regamey, B., Martin, S., Kummert, M., Schoeneich, P., & Reynard, E. (2012). The ArcGIS version of the geomorphological mapping legend of the University of Lausanne. http://unil.ch/igd/legende_UNIL

Lilleøren, K. S., Etzelmüller, B., Gärtner-Roer, I., Kääb, A., Westermann, S., & Gumundsson, Á. (2013). The distribution, thermal characteristics and dynamics of permafrost in Tröllaskagi, Northern Iceland, as inferred from the distribution of rock glaciers and ice-cored moraines. *Permafrost and Periglacial Processes*, *24*(4), 322–335. https://doi.org/10.1002/ppp.1792

Martin, H. E., Whalley, W. B, & Caseldine, C. (1991). Glacier fluctuations and rock glaciers in Tröllaskagi, Northern Iceland, with special reference to 1946–1986. In J. K. Maizels, & C. Caseldine (Eds.), *Environmental Change in Iceland: Past and Present* (pp. 255–265).

Netherlands: Springer. https://doi.org/10.1007/978-94-011-3150-6_17

Mercier, D., Cossart, E., Decaulne, A., Feuillet, T., Jónsson, H. P., & Sæmundsson, Þ. (2013). The Höfðahólar rock avalanche (sturzström): chronological constraint of paraglacial landsliding on an Icelandic hillslope. *The Holocene*, *23*(3), 432–446. https://doi.org/10.1177/0959683612463104

Mertes, J. R., Gulley, J. D., Benn, D. I., Thompson, S. S., & Nicholson, L. I. (2017). Using structure-from-motion to create glacier DEMs and orthoimagery from historical terrestrial and oblique aerial imagery: SfM on differing historical glacier imagery sets. *Earth Surface Processes and Landforms*, *42*(14), 2350–2364. https://doi.org/10.1002/esp.4188

Micheletti, N., Chandler, J. H., & Lane, S. N. (2014). Investigating the geomorphological potential of freely available and accessible structure from motion photogrammetry using a smartphone. *Earth Surface Processes and Landforms*, *40*(4), 473–486. https://doi.org/10.1002/esp.3648

Micheletti, N., Chandler, J. H., & Lane, S. N. (2015). Structure from motion (SfM) photogrammetry. British Society for Geomorphology. Geomorphological Techniques, Cap. 2, Sec. 2.2. Online Edition (ISSN 2047-0371). https://www.geomorphology.org.uk/sites/default/files/geom_tech_chapters/2.2.2_sfm.pdf

Midgley, N. G., & Tonkin, T. N. (2017). Reconstruction of former glacier surface topography from archive oblique aerial images. *Geomorphology*, *282*, 18–26. https://doi.org/10.1016/j.geomorph.2017.01.008

Monnier, S., & Kinnard, C. (2015). Reconsidering the glacier to rock glacier transformation problem: New insights from the central Andes of Chile. *Geomorphology*, *238*, 47–55. https://doi.org/10.1016/j.geomorph.2015.02.025

Monnier, S., & Kinnard, C. (2016). Pluri-decadal (1955–2014) evolution of glacier–rock glacier transitional landforms in the central Andes of Chile (30–33° S). *Earth Surface Dynamics*, *5*(3), 493–509. https://doi.org/10.5194/esurf-5-493-2017

Monnier, S., Kinnard, C., Surazakov, A., & Bossy, W. (2014). Geomorphology, internal sctructure, and successive development of a glacier foreland in the semiarid Chilean Andes (Cerro Tapado, upper Elqui Valley, 30° 08′ S., 69° 55′ W). *Geomorphology*, *207*, 126–140. https://doi.org/10.1016/j.geomorph.2013.10.031

Peña Monné, J. L., Pellicer Corellano, F., Chueca Cía, J., & Julián Andrés, A. (1997). Leyendas para mapas geomorfológicos a escalas 1:100.000/1:200.000 y 1:25.000/1:50.000. In J. L. Peña Monné (Ed.), *Cartografía geomorfológica básica y aplicada* (pp. 127–143). Geoforma Ediciones. https://geomorfologia.es/sites/default/files/Pe%C3%B1a%201997%20Cartograf%C3%ADa%20Geomorfol%C3%B3gica.pdf

Sæmundsson, K., Kristjansson, L., McDougall, I., & Watkins, N. D. (1980). K-Ar dating, geological and paleomagnetic study of a 5-km lava succession in northern Iceland. *Journal of Geophysical Research Solid Earth*, *85*(B7), 3628–3646. https://doi.org/10.1029/JB085iB07p03628

Sæmundsson, Þ., Morino, C., Helgason, J. K., Conway, S. J., & Pétursson, H. G. (2018). The triggering factors of the Móafellshyrna debris slide in northern Iceland: Intense precipitation, earthquake activity and thawing of mountain permafrost. *Science of the Total Environment*, *621*, 1163–1175. https://doi.org/10.1016/J.SCITOTENV.2017.10.111

Tanarro, L. M., Palacios, D., Andrés, N., Fernández-Fernández, J. M., Zamorano, J. J., Sæmundsson, Þ, & Brynjólfsson, S. (2019). Unchanged surface morphology in debris-covered glaciers and rock glaciers in Tröllaskagi peninsula (northern Iceland). *Science of the Total Environment*, *648*, 218–235. https://doi.org/10.1016/j.scitotenv.2018.07.460

Tanarro, L. M., Palacios, D., Zamorano, J. J., & Andrés, N. (2018). Proposal for geomorphological mapping of debris-covered and rock-glaciers and its application to Tröllaskagi Peninsula (Nothern Iceland). *Journal of Maps*, *14*(2), 692–703. https://doi.org/10.1080/17445647.2018.1539417

Tricart, J. (1976). *Legende pour la carte geomorphologique de la France au 1:50.000*. Centre National de la Reserche Scientifique (C.N.R.S.).

Wangensteen, B., Gudmundsson, Á, Eiken, T., Kääb, A., Farbrot, H., & Etzelmüller, B. (2006). Surface displacements and surface age estimates for creeping slope landforms in Northern and Eastern Iceland using digital photogrammetry. *Geomorphology*, *80*(1–2), 59–79. https://doi.org/10.1016/j.geomorph.2006.01.034

Whalley, W. B., Douglas, G. R., & Jonsson, A. (1983). The magnitude and frequency of large rockslides in Iceland in the postglacial. *Geografiska Annaler Series A Physical Geography*, *65*(1-2), 99–110. https://doi.org/10.2307/520724